ORIGINAL ARTICLE

Novel antiangiogenic therapy targeting biglycan using tumor endothelial cell-specific liposomal siRNA delivery system

Nako Maishi[1,2,3] | Yu Sakurai[4,5] | Hiroto Hatakeyama[4,6] | Yui Umeyama[1] | Takashi Nakamura[4] | Rikito Endo[4] | Mohammad Towfik Alam[1,2,3] | Cong Li[1] | Dorcas Akuba-Muhyia Annan[1,2] | Hiroshi Kikuchi[2,7] | Hirofumi Morimoto[2] | Masahiro Morimoto[1,2,8] | Kosuke Akiyama[3] | Noritaka Ohga[3,8] | Yasuhiro Hida[9] | Hideyoshi Harashima[4] | Kyoko Hida[1,2,3]

[1]Vascular Biology and Molecular Pathology, Hokkaido University Graduate School of Dental Medicine, Sapporo, Japan

[2]Vascular Biology, Frontier Research Unit, Institute for Genetic Medicine, Hokkaido University, Sapporo, Japan

[3]Department of Vascular Biology, Hokkaido University Graduate School of Dental Medicine, Sapporo, Japan

[4]Faculty of Pharmaceutical Sciences, Hokkaido University, Sapporo, Japan

[5]Membrane Transport and Drug Targeting Laboratory, Graduate School of Pharmaceutical Sciences, Tohoku University, Sendai, Japan

[6]Graduate School of Pharmaceutical Sciences, Chiba University, Chiba, Japan

[7]Department of Renal and Genitourinary Surgery, Hokkaido University Graduate School of Medicine, Sapporo, Japan

[8]Department of Oral Diagnosis and Medicine, Hokkaido University Graduate School of Dental Medicine, Sapporo, Japan

[9]Department of Cardiovascular and Thoracic Surgery, Faculty of Medicine, Hokkaido University, Sapporo, Japan

Correspondence
Kyoko Hida, Vascular Biology and Molecular Pathology, Hokkaido University Graduate School of Dental Medicine, Sapporo 060-8586, Japan.
Email: khida@den.hokudai.ac.jp

Funding information
This research was supported by JSPS Grants-in-Aid for Scientific Research to NM (JP21K10107), HK (JP19K18549), YH (JP21H03019), and KH (JP21H04840), Grants from Japan Agency for Medical Research and Development (AMED) to NM (JP18ck0106198h0003) and KH (JP20ck0106406h0003).

Abstract

Tumor blood vessels play important roles in tumor progression and metastasis. Targeting tumor endothelial cells (TECs) is one of the strategies for cancer therapy. We previously reported that biglycan, a small leucine-rich proteoglycan, is highly expressed in TECs. TECs utilize biglycan in an autocrine manner for migration and angiogenesis. Furthermore, TEC-derived biglycan stimulates tumor cell migration in a paracrine manner leading to tumor cell intravasation and metastasis. In this study, we explored the therapeutic effect of biglycan inhibition in the TECs of renal cell carcinoma using an *in vivo* siRNA delivery system known as a multifunctional envelope-type nanodevice (MEND), which contains a unique pH-sensitive cationic lipid. To specifically deliver MEND into TECs, we incorporated cyclo(Arg–Gly–Asp–D–Phe–Lys) (cRGD) into MEND because $\alpha_V\beta_3$ integrin, a receptor for cRGD, is selective and highly expressed in TECs. We developed RGD-MEND-encapsulating siRNA against biglycan. First, we confirmed that MEND was delivered into OS-RC-2 tumor-derived TECs and induced *in vitro* RNAi-mediated gene silencing. MEND was then injected intravenously into OS-RC-2 tumor-bearing mice. Flow cytometry analysis demonstrated

Abbreviations: DT, Diphtheria toxin; EC, Endothelial cells; EGF, Epidermal growth factor; EGFR, Epidermal growth factor receptor; MEND, Multifunctional envelope-type nano device; NEC, Normal endothelial cells; TEC, Tumor endothelial cells; VEGF, Vascular endothelial growth factor.

that MEND was specifically delivered into TECs. Quantitative RT-PCR indicated that biglycan was knocked down by biglycan siRNA-containing MEND. Finally, we analyzed the therapeutic effect of biglycan silencing by MEND in TECs. Tumor growth was inhibited by biglycan siRNA-containing MEND. Tumor microenvironmental factors such as fibrosis were also normalized using biglycan inhibition in TECs. Biglycan in TECs can be a novel target for cancer treatment.

KEYWORDS

biglycan, drug delivery system, tumor angiogenesis, tumor endothelial cell, tumor microenvironment

1 | INTRODUCTION

Angiogenesis, the formation of new blood vessels, plays a vital role in tumor progression. Angiogenic factors such as VEGF are released from tumor cells and other stromal cells to stimulate the formation of new capillaries for tumorigenesis. Without angiogenesis, tumors remain dormant at diameters of 1–2 mm.[1] Dr. Folkman proposed antiangiogenic therapy as an anticancer therapy.[2] The important targets of antiangiogenic therapy are TECs, which line the inner surface of tumor blood vessels. Anti-VEGF drugs such as bevacizumab, which is a humanized anti-VEGF monoclonal antibody,[3] have become successful therapeutics and have improved clinical outcomes. However, as VEGF signaling is also required in normal physiologic angiogenesis, anti-VEGF agents have several adverse effects.[4] Therefore, understanding TEC biology is essential for developing novel antiangiogenic drugs that specifically target TECs with less harmful effects on NECs.

In the past two decades, it has been reported that TECs exhibited some abnormal phenotypes compared with NECs.[5] For instance, NEC and TEC gene expression patterns are different.[6-11] TECs proliferate and migrate faster than NECs.[12,13] Several upregulated genes in TECs are associated with angiogenesis.[11,14-18] Targeting these molecules may serve as a novel antiangiogenic therapy.

Biglycan, a member of the small leucine-rich proteoglycan family, exists in the ECM as a matrix component and an essential signaling molecule.[19] It is also known as a damage-associated molecular pattern. Secreted biglycan binds with Toll-like receptor 2 (TLR2) and TLR4 on immune cells such as macrophages, causing an inflammatory response through the nuclear factor-kappa B (NF-κB) pathway.[20] We previously observed that biglycan expression was upregulated in TECs of several types of tumors such as melanoma[14,21] and breast cancer[22] in the murine model and renal, lung, colon, and liver cancers in human clinical cases.[14,21] TECs utilize biglycan in an autocrine manner for migration through TLRs.[14] Biglycan secreted from TECs actively promoted tumor cell intravasation in a paracrine manner and caused distant metastasis.[21] Therefore, biglycan in TECs is a potential target for cancer therapy. However, no biglycan inhibitors, including compounds and neutralizing antibodies, are commercially available.

RNAi is a useful tool for target-specific inhibition because it regulates target genes in a sequence-dependent manner. *In vivo* delivery of siRNA to the target organ is potentially a powerful tool for therapeutic applications.[23] However, siRNA delivery requires several carriers such as nanodrug delivery systems (DDSs) because siRNA is rapidly degraded in the body.[24] Nano DDSs can target the blood vessels of tumor tissues as they can target an organ using functional devices.[25] We previously developed a liposomal siRNA system known as the multifunctional envelope-type nanodevice (MEND).[26-29] We incorporated cyclo(Arg–Gly–Asp–D–Phe–Lys) (cRGD) into MEND to specifically target TECs because $\alpha_V\beta_3$ integrin, a cRGD receptor, is selectively expressed in TECs at high levels.[30] This RGD-MEND was used to specifically deliver siRNA into tumor blood vessels.[31] VEGFR2 silencing using the TEC-targeting RGD-MEND induced antiangiogenic effect and antitumor effect.[31,32] In this study, this TEC-targeting RGD-MEND was used to investigate the therapeutic effect of biglycan inhibition in TECs.

2 | MATERIALS AND METHODS

2.1 | Isolation of TECs and NECs and cell culture

The human renal clear cell carcinoma cell line OS-RC-2 was purchased from the RIKEN Cell Bank (Tsukuba, Japan) and cultured in RPMI1640 medium (Sigma-Aldrich, St. Louis, MO, USA) supplemented with 10% heat-inactivated FBS. The TECs and NECs used in this study had been previously isolated.[10-12,15,16,33-36] Subcutaneously xenografted OS-RC-2 tumors grown in nude mice were minced and digested using collagenase II (Gibco Thermo Fisher Scientific, Inc., Waltham, MA, USA). After removing the blood cells using a lysing buffer (BD Biosciences, San Jose, CA, USA), the ECs were sorted through a magnetic cell sorting system (Miltenyi Biotec, Bergisch Gladbach, Germany) using anti-CD31 microbeads according to the manufacturer's instructions, followed by incubation with an Fc receptor (FcR) blocking reagent (Miltenyi). The ECs in the kidney tissue and dermis of nontumor-bearing mice were also sorted as NECs. The ECs were maintained in EGM-2 MV (Lonza, Basel, Switzerland) containing 15% FBS. Diphtheria toxin (DT; Calbiochem)

was added to the EC subcultures to eliminate any remaining human tumor cells that expressed heparin-binding EGF-like growth factor, a DT receptor. The isolated ECs were further purified through a second round of purification using FITC-conjugated *Bandeiraea simplicifolia* isolectin (BSI-B4 lectin) (Vector Laboratories, Burlingame, CA, USA). These cells were cultured at 37°C in a humidified atmosphere containing 5% CO_2. PCR was used to check the absence of *Mycoplasma pulmonis*. To analyze biglycan expression in the cells of OS-RC-2 tumor tissue, a single-cell preparation was performed as described above. A portion of the cells was cytospun onto glass slides, fixed in 4% paraformaldehyde (PFA) for 10 min, permeabilized with 0.15% Triton X-100, and blocked with 2% goat and 5% sheep serum for 1 h, for immunostaining. The cells were incubated with anti-CD31 (BioLegend) and anti-biglycan (Kerafast) antibodies as primary antibodies, followed by Alexa Fluor 568-conjugated goat anti-rat IgG (Invitrogen) and Alexa Fluor 647-conjugated goat anti-rabbit IgG (Invitrogen), as secondary antibodies. Biglycan-positive cell rate in total ($N = 708$) and CD31-positive cell rate in the biglycan-positive cells were calculated under a BZ-X810 microscope equipped with BZ-X800 Analyzer software (Keyence Corporation, Itasca, IL, USA). Another portion of the single cells of OS-RC-2 tumors was incubated with FITC-conjugated anti-CD45 (BioLegend) and allophycocyanin (APC)-conjugated anti-CD31 (BioLegend) antibodies to isolate $CD31^-CD45^-$ and $CD31^-CD45^+$ cell populations using the FACS Aria II system (Becton Dickinson). Data were analyzed using FlowJo software (Tree Star Inc.).

2.2 | RNA isolation, RT-PCR, and quantitative PCR

Total RNA was extracted using the ReliaPrep™ RNA Cell Miniprep System (Promega, Madison, WI, USA), according to the manufacturer's instructions. cDNA was synthesized using ReverTra-Plus (Toyobo) and amplified using PCR. Quantitative real-time RT-PCR (qRT-PCR) was performed using a KAPA SYBR® FAST qPCR Kit (KAPA Biosystems, Boston, MA, USA). The cycling conditions were established based on CFX Manager (Bio-Rad). The biglycan mRNA expression levels were normalized to those of GAPDH, β-actin (Actb), or CD31 and analyzed using the $2^{-\Delta\Delta Ct}$ method. The following primers were used: human ACTB forward 5′-TACAGGAAGTCCCTTGCCATCC-3′ and reverse 5′-AAGCAATGCTATCACCTCCCCTG-3′, human BGN forward 5′-GAGAGGCTTCTGGGACTTCA-3′ and reverse 5′-AGGTGGGTG TGACAGAGTCC-3, mouse Gapdh forward 5′-TCTGACGTGCCG CCTGGAG-3′ and reverse 5′-TCGCAGGAGACAACCTGGTC-3′, mouse Actb forward 5′-TTTGCACATGCCGGAGCCGTTG-3′ and reverse 5′-TTTGCAGCTCCTTCGTTGCCGG-3′, mouse CD31 forward 5′-CAGAGCGGATAATTGCCATTCC-3′ and reverse 5′- ACAGGA TGGAAATCACAACTTCATC-3′, and mouse biglycan forward 5′-AA CTCACTGCCCCACCACAGCTTC-3′ and reverse 5′-GCGGTGGCA GTGTGCTCTATCCATC-3′, mouse Cd51 forward 5′-GTGTGAGGAA CTGGTCGCCT-3′ and reverse 5′-TATGAGCCTGCCGACTGACG-3′, mouse Cd61 forward 5′-GACAGGATGCGAGCGCAGTG-3′ and reverse 5′-GGGTGAGCCCTGAGACAAAGT-3′.

2.3 | ELISA

The plasma of OS-RC-2 tumor-bearing mice was collected every 7th day after tumor cell injection. Tumor-free normal mouse plasma was used as the normal control. Plasma biglycan concentrations in mice were evaluated using mouse biglycan ELISA kit (Cloud-Clone Corp., Houston, TX, USA).

2.4 | Analysis of integrin $\alpha_V\beta_3$ expression using flow cytometry

Cells were incubated with phycoerythrin (PE)-conjugated anti-CD51/integrin α_V (BioLegend) and APC-conjugated anti-CD61/integrin β_3 (BioLegend) antibodies, respectively, and analyzed using the FACS Aria II system. Data were analyzed using FlowJo software. Each fluorophore-conjugated isotype control was used as the negative control.

2.5 | Preparation of RGD-MEND

RGD-MEND was prepared as described previously.[31,37,38] A pH-sensitive cationic lipid, YSK05, was synthesized as described previously.[28] Briefly, 40–160 μg siRNA solution in 200 μl citrate buffer (2 mM, pH 4.0) was added to 400 μl of 90% tertiary butanol (t-BuOH/double-distilled water (v/v)) containing 1500 nmol YSK05, 1500 nmol cholesterol, and 45 nmol PEG-DMG (1.5 mol% of total lipid) and mixed step by step. Unencapsulated siRNA and t-BuOH were removed from the mixture diluted with PBS using Amicon Ultra-15 (Merck Millipore, Darmstadt, Germany), according to the manufacturer's instructions. The encapsulation efficiency and recovery rate of siRNA were checked by RiboGreen assay.[31,37,39] cRGD was conjugated to PEG-DSPE using *N*-hydroxysuccinimide (RGD-PED-DSPE) to display an RGD peptide on the surface of MEND, as previously described.[31,37] To modify MEND with RGD-PEG-DSPE (RGD-MEND), it was mixed with 3 mol% of PEG-DSPE in 7.5% ethanol (EtOH; v/v) solution (2 mM citrate buffer, pH 5.5) and then centrifuged in an Amicon Ultra-15 concentrator to remove the remaining EtOH. When MEND was labeled with a fluorescent dye, 0.5 mol% of DiI, 1,1′-dioctadecyl-3,3,3′,3′-tetramethylindocarb ocyanine perchlorate or DiD, 1,1-dioctadecyl-3,3,3,3-tetramethylin dodicarbocyanine was added to the initial lipid solution. The siRNA against biglycan (sense, 5′-gaacauagccagaugaagaTT-3′ and antisense, 5′-ucuucaucuggcuauguucTT-3′) was purchased from Cosmo Bio Co., Ltd. (Tokyo, Japan).

2.6 | Animal model

Seven-week-old female nude mice (BALB/c AJcl-nu/nu, CLEA Japan) were housed under specific pathogen-free conditions. In total, 1×10^6 OS-RC-2 cells in HBSS (Gibco® Thermo Fisher Scientific) were

implanted subcutaneously in the right flanks of nude mice. The OS-RC-2-bearing mice were administered intravenously 4 mg/kg DiI-labeled RGD-MEND on days 15 and 16 when the tumor volume reached 200 mm^3 to evaluate MEND uptake and gene silencing in TECs. Tumor tissues were excised 24 h after the second MEND injection. The OS-RC-2-bearing mice were administered intravenously with 3 mg/kg scramble siRNA-containing RGD-MEND (Scr siRNA-MEND) or biglycan siRNA-containing RGD-MEND (Bgn siRNA-MEND) twice a week for 3 weeks beginning on day 7 to evaluate the therapeutic effects of MEND. The tumor tissues were excised on day 28. All procedures for animal care and experimentation were approved by the Hokkaido University Animal Committee and conducted according to institutional guidelines and approved guidelines.

2.7 | Evaluation of MEND uptake using flow cytometry and fluorescence microscopy

Cells were incubated with DiD-labeled Scr siRNA-MEND or Bgn siRNA-MEND at the indicated dose for 3 h to investigate MEND uptake in OS-RC-2-ECs *in vitro*. The cells were then collected with trypsin–EDTA and analyzed using a FACS Aria II system. Data were analyzed using FlowJo software. Cells were washed with PBS, fixed in 4% PFA, and counterstained with DAPI (Dojin, Kumamoto, Japan) for fluorescence microscopy. Sample images were acquired using an FV1000 confocal microscope equipped with the Fluoview FV10-ASM Viewer software. To analyze the MEND uptake in tissue, AlexaFluor 647-conjugated GSL-IB4 lectin (2 mg/kg, Thermo Fisher Scientific) was injected intravenously via the tail vein to stain functional blood vessels 10 min before tumor resection. A portion of the excised OS-RC-2 tumor tissue was immersed in FITC-conjugated BSI-B4 to visualize blood vessels, and images were acquired using an FV1000 confocal microscope to further investigate MEND localization *in vivo*. Another portion of the excised tumor tissue or normal kidney and skin tissue of the tumor-bearing mice were minced and digested using collagenase II. Cells were incubated with FITC-conjugated anti-CD34 (eBioscience® Thermo Fisher Scientific) and APC-conjugated anti-CD45 (BioLegend) antibodies, or APC-conjugated anti-CD31 (BioLegend) and FITC-conjugated anti-CD45 (BioLegend) antibodies after removing the blood cells using a lysing buffer and were analyzed using the FACS Aria II. Data were analyzed using FlowJo software.

2.8 | Histological analysis

Resected OS-RC-2 tumor tissues were fixed in formalin, paraffin-embedded, and 4-μm thick sections were prepared for H&E staining to perform histopathological examination. The tumor tissues were dissected and embedded in optimal cutting temperature (OCT) compound (Sakura Finetek Co., Torrance, CA), immediately immersed in liquid nitrogen, and cut into 10-μm-thick sections using a cryostat (Leica CM3050S, Leica Biosystems, Wetxlar, Germany). The frozen

sections were fixed in 100% ice-cold acetone for 30 min, permeabilized with 0.1% Triton X-100, and blocked with 5% goat serum for 1 h for double staining of CD31 and biglycan. The sections were incubated with rabbit anti-biglycan (Kerafast) for 2 h, Alexa Fluor 488-conjugated goat anti-rabbit IgG (Invitrogen) for 1 h, and Alexa Fluor 647-conjugated anti-mouse CD31 (BioLegend) for 2 h. The frozen sections were fixed in 4% PFA for 30 min, permeabilized with 0.1% Triton X-100, and blocked with 5% goat serum for 1 h for double staining of CD31 and α-smooth muscle actin (α-SMA). The sections were incubated with rat anti-mouse CD31 (BD Biosciences) and rabbit anti-α-SMA (Abcam) for 16 h and Alexa Fluor 647-conjugated goat anti-rat IgG (BioLegend) and Alexa Fluor 488-conjugated goat anti-rabbit IgG (Invitrogen) for 2 h. The frozen sections were fixed in cold methanol for 30 min and blocked with 5% goat serum for 1 h for staining of glucose transporter 1 (GLUT1). The sections were incubated with rabbit anti-GLUT1 (Abcam) for 16 h and Alexa Fluor 647-conjugated goat anti-rabbit IgG (Thermo Fisher Scientific) for 1 h. This was followed by counterstaining with DAPI, after which sample images were acquired using an FV1000 confocal microscope equipped with Fluoview FV10-ASM Viewer software or a BZ-X810 microscope equipped with BZ-X800 Analyzer software. The area of CD31-positive cells was determined using ImageJ software (NIH), and microvessel density (MVD) was calculated as a percentage of the CD31-positive area to the total area. Tip-like endothelial sprouts, defined as tapered endothelial processes that extended from the main axis of vessels, were counted in CD31 staining images as previously described.[40,41] The pericyte coverage was calculated using the ratio of the number of α-SMA- and CD31-double-positive blood vessels to the number of total CD31-positive blood vessels. The GLUT1 staining area was estimated as the hypoxia area using ImageJ software. To assess perfused blood vessels using siRNA-RGD-MEND treatment, FITC-conjugated BSI-B4 lectin (2 mg/kg) was intravenously injected via the tail vein to stain functional blood vessels. Tumors were extracted 10 min after injection, followed by immersion in Dylight649-conjugated GSL-IB4 lectin (Vector Laboratories) to stain all blood vessels. Images were acquired using a BZ-X810 microscope equipped with BZ-X800 Analyzer software. The rate of the double-positive area in the GSL-IB4 lectin-stained area was calculated as functional blood vessels. Azan staining was performed using azocarmine combined with a counterstain incorporated with aniline blue and orange G after mordanting with phosphotungstic acid. Azan staining was used to evaluate connective tissues with which the cytoplasm was stained orange and the collagen fibers were stained blue. The slides were digitally scanned using NanoZoomer and viewed using the NDP.view2 viewing software (Hamamatsu Photonics, Hamamatsu, Japan). The blue range was analyzed as the collagen area using ImageJ software.

2.9 | Statistical analysis

All data were expressed as mean ± standard deviation. Box and whisker plots represented median (centerline), 25th and 75th

percentiles (box), and minimum and maximum (whiskers). Student's *t* test was used for comparing two groups. The Kruskal–Wallis test was performed for multiple comparisons, followed by the Wilcoxon test for paired comparisons. A value of *p* < 0.05 was considered to indicate a statistically significant difference, which was a representative of three independent experiments. Statistical analysis was conducted using JMP version 13 (SAS Institute, Tokyo, Japan).

3 | RESULTS

3.1 | Biglycan expression in TECs of renal cell carcinoma

We previously reported that tumor blood vessels in human renal cell carcinoma expressed higher biglycan levels comparted to those of their normal counterparts.[14] In this study, a renal cell carcinoma model, that is, OS-RC-2, was adopted to explore the effects of biglycan inhibition on TECs. First, biglycan expression was evaluated in OS-RC-2 tumor tissues using immunohistochemistry. Double staining of biglycan and CD31, an EC marker, demonstrated that biglycan was stained in tumor tissues, and some parts were co-stained with CD31 (Figures 1A and S1A). These data suggested that biglycan is expressed in tumor blood vessels and other stromal cells. Next, to evaluate biglycan-expressing cell populations in the tumors, we checked the biglycan expression in OS-RC-2 tumor cells by PCR *in vitro*. OS-RC-2 tumor cells did not exhibit biglycan expression (Figure S1B). Furthermore, cells in OS-RC-2 tumor tissue were cytospun onto glass slides and stained with anti-biglycan and CD31 antibodies. Some cells, including CD31-positive cells, revealed
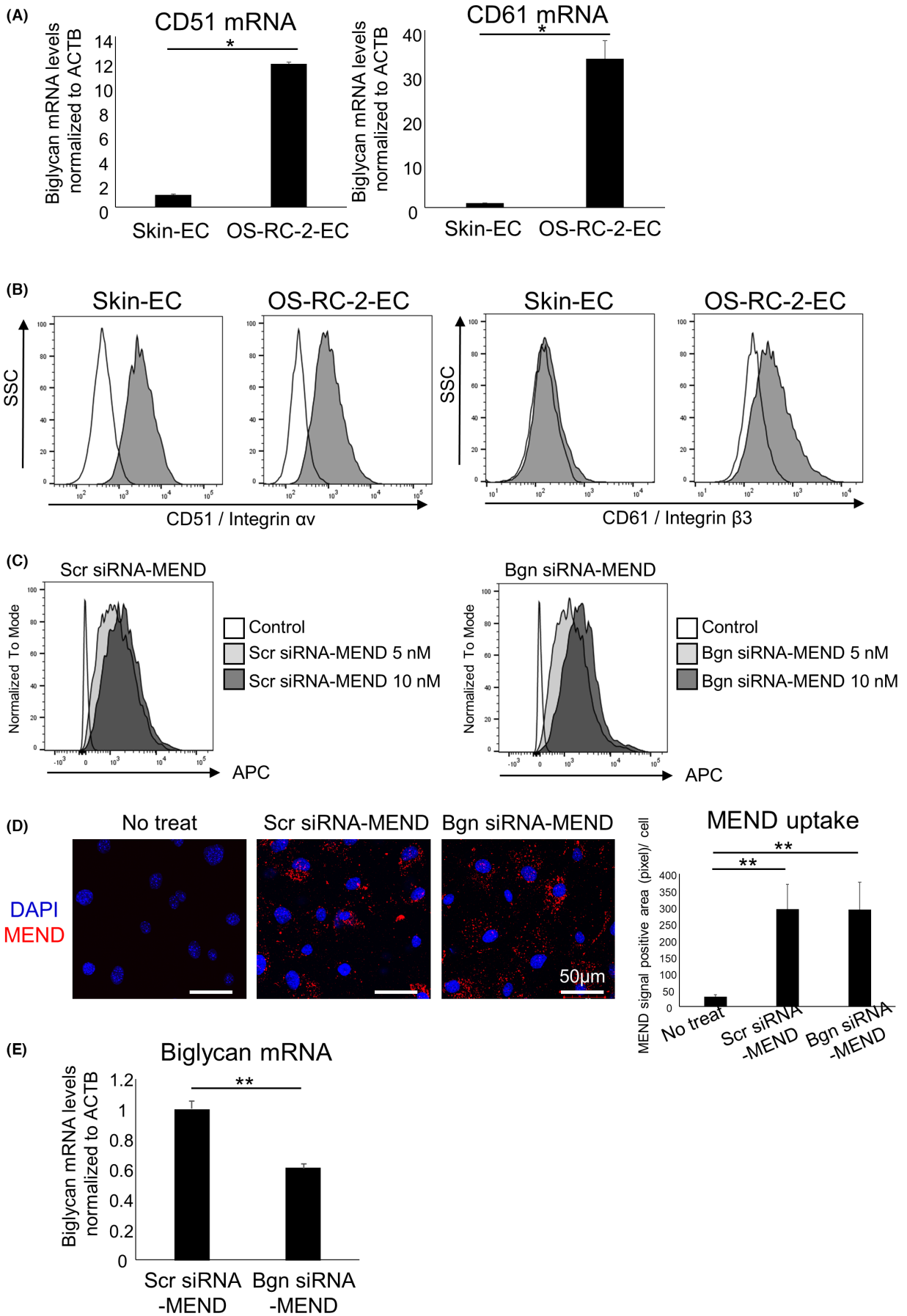
biglycan expression (Figure S1C). Cells in the tumor tissue (33%) were positive for biglycan and 78.1% of the biglycan-positive cells were CD31-positive cells, that is, ECs (Figure S1D). In CD31-negative cells, CD45-negative cells but not CD45-positive cells exhibited biglycan expression (Figure S1E,F), suggesting some stromal cells, such as fibroblasts, express biglycan, which is consistent with previous reports.[42,43] We isolated TECs from OS-RC-2 tumor tissues (OS-RC-2-EC) as described previously.[10,33] Compared with normal ECs derived from skin tissues (Skin-EC) or kidney tissues (Kidney-EC), OS-RC-2-ECs showed high biglycan expression (Figure 1B). These data suggest that biglycan is highly expressed mainly in TECs of OS-RC-2 tumor tissue. As biglycan is a secreted protein, we next analyzed over time its secretion levels in the plasma of OS-RC-2 tumor-bearing mice. Plasma biglycan levels were increased in these mice, depending on tumor growth and metastasis (Figures 1C and S2A,B). These data suggested that TECs in OS-RC-2 express and secrete high biglycan levels.

3.2 | Evaluation of gene silencing by MEND *in vitro*

We used MEND, an siRNA delivery system, to examine the therapeutic effect of biglycan inhibition in the TECs of renal cell carcinoma *in vivo*. To specifically deliver it into TECs, we incorporated cRGD because $\alpha_V\beta_3$ integrin, a cRGD receptor, is selectively expressed in TECs at high levels.[30] We confirmed the expressions of integrin α_V and β_3 in OS-RC-2-ECs using PCR and flow cytometry. $\alpha_V\beta_3$ integrin (CD51 and CD61) were highly expressed in OS-RC-2-ECs compared with Skin-ECs (Figure 2A,B). We developed RGD-MEND-encapsulating biglycan siRNA. First, we confirmed MEND uptake
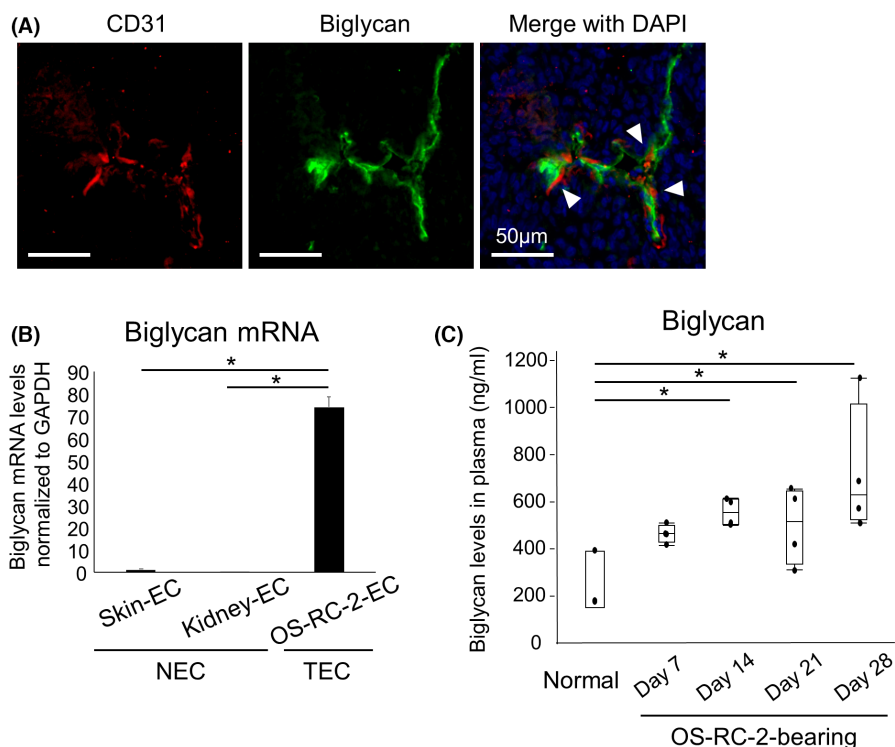
FIGURE 1 TECs in OS-RC-2 tumors highly express biglycan. (A) Biglycan expression in OS-RC-2 tumor tissues was analyzed by immunohistochemistry. Arrowheads indicate CD31 and biglycan colocalization. Scale bars, 50 μm. (B) Biglycan expression in each endothelial cell (EC) was evaluated by qRT-PCR (*p* < 0.01 versus OS-RC-2-ECs, Kruskal–Wallis test, followed by Wilcoxon test. Data are presented as mean ± SD, *n* = 4 qRT-PCR runs). (C) Plasma biglycan levels were determined by ELISA for each mouse group (*p* < 0.01 versus normal, two-tailed Student's *t* test; *n* = 4–5 mice per group)

(A)

CD51 mRNA

CD61 mRNA

(B)

CD51 / Integrin αv

CD61 / Integrin β3

(C)

Scr siRNA-MEND

Bgn siRNA-MEND

(D)

No treat   Scr siRNA-MEND   Bgn siRNA-MEND

DAPI
MEND

50μm

MEND uptake

(E)

Biglycan mRNA

FIGURE 2 Uptake and gene silencing by MEND in OS-RC-2-ECs were evaluated *in vitro*. (A) CD51 (integrin α_V) and CD61 (integrin β_3) mRNA expression in each EC was evaluated by qRT-PCR (*$p < 0.01$, two-tailed Student's *t* test. Data are presented as mean $\pm$ SD, $n = 4$ qRT-PCR runs). (B) Representative flow cytometry of CD51 and CD61 in Skin-ECs and OS-RC-2-ECs (gray area). The white area shows the IgG isotype control. (C) Representative flow cytometric analysis of OS-RC-2-ECs treated with each fluorophore-labeled MEND at the indicated dose for 3 h showing light and dark gray expression areas. Each EC group treated with vehicle was used as a control (white area). (D) Fluorescent signals of OS-RC-2ECs treated with each MEND at 10 nM for 3 h were detected using a confocal microscope. The right panel shows the quantitative MEND signal positive area (*$p < 0.01$ versus no treatment, Kruskal–Wallis test, followed by Wilcoxon test. Data are presented as mean $\pm$ SD, $n = 30$). (E) Biglycan expression was evaluated by qRT-PCR after treatment of each siRNA at 10 nM for 24 h (*$p < 0.01$, two-tailed Student's *t* test. Data are presented as mean $\pm$ SD, $n = 4$ qRT-PCR runs)

into OS-RC-2-ECs *in vitro*. To visualize MEND, it was labeled with DiI. Flow cytometric analysis revealed that DiI-labeled Bgn siRNA-MEND was delivered into OS-RC-2-ECs in a dose-dependent manner similar to Scr siRNA-MEND (Figure 2C). MEND signals were also detected using confocal microscopy (Figure 2D). We next evaluated the RNAi-mediated gene silencing using qRT-PCR. Biglycan mRNA expression was inhibited by Bgn siRNA-MEND (Figure 2E).

3.3 | Selective delivery of MEND into tumor blood vessels after systemic injection

MEND was injected intravenously into OS-RC-2 tumor-bearing mice to confirm whether RGD-MEND was selectively delivered into tumor blood vessels. DiI-labeled MEND signals were detected in the tumor tissues of each MEND-treated group using an *in vivo* imaging system (Figures 3A and S3A). To assess MEND localization in the tumor tissues, the blood vessels of the resected OS-RC-2 tumors were visualized using fluorophore-conjugated lectin. Alexa Fluor 647-conjugated GSL-IB4 lectin was injected via the tail vein to stain functional blood vessels, followed by immersion of the tumors in FITC-conjugated BSI-B4 lectin to stain all blood vessels, including nonfunctional ones. Under the confocal microscope, the MEND signals were found to be colocalized with lectin (Figures 3B and S3B). We also analyzed MEND uptake in the TECs of OS-RC-2. After DiI-labeled siRNA-MEND injection via the tail vein, tissues were resected and homogenized, and then DiI-MEND signals were detected using flow cytometry. The CD34+CD45− EC population showed DiI-labeled MEND signals (Figure 3C), suggesting that MEND was delivered into TECs. Biglycan mRNA knockdown in TECs by Bgn siRNA-MEND was also confirmed by qRT-PCR (Figure 3D). To assess the specificity of siRNA-MEND delivery to TECs, we also analyzed the biodistributions of siRNA-MEND in normal organs of the tumor-bearing mice. MEND signals were hardly detected in normal kidney and skin tissues (Figure S3A). Additionally, MEND signals in ECs of kidney and skin tissues were low compared with those of tumor tissue (Figure S3C).

## 3.4 | Therapeutic effect of Bgn siRNA-MEND

Finally, we examined the therapeutic effect of biglycan inhibition by Bgn siRNA-MEND treatment. MEND administration was started 7 days after tumor injection, when the tumors were visible.

Figure 4A shows the time course of MEND injection. No significant difference of body weight changes was observed between the two groups (Figure 4B). The surface of the resected tumors in the Bgn siRNA-MEND group appeared smoother than that of the Scr siRNA-MEND group when the resected tumors were observed. Moreover, tumor congestion was improved by Bgn siRNA-MEND treatment (Figure 4C). Bgn siRNA-MEND treatment reduced biglycan expression in the tumors, especially in blood vessels (Figure S4A). Bgn siRNA-MEND treatment significantly inhibited tumor growth compared with the control group (Figures 4D and S4B), suggesting that biglycan in TECs is essential for tumor progression. We also evaluated the therapeutic effects of Bgn siRNA-MEND on the tumor microenvironment. We visualized the blood vessels in these tumors by immunohistochemistry (Figure 5A) as we reported previously that biglycan in TECs is involved in tumor angiogenesis.[14] We found morphological differences between the two groups. The blood vessels in the tumors treated with Bgn siRNA-MEND showed smoother morphology and had fewer sprouts. MVD and tip-like endothelial sprouting were decreased due to biglycan inhibition (Figure 5B,C). These data suggested that biglycan inhibition can cause an antiangiogenic effect, which is consistent with our previous finding through an *in vitro* study using siRNA[14] and an *in vivo* study using biglycan knockout mice.[22] Pericyte coverage was also analyzed using immunostaining to evaluate blood vessel maturation. The proportion of pericyte-covered blood vessels was increased due to Bgn siRNA-MEND treatment (Figure 5D,E). It is known that an increase in the proportion of pericyte-covered mature blood vessels improves blood perfusion. Therefore, we next analyzed the function of blood vessels with lectin injection. As expected, the blood perfusion was increased in the tumor of the Bgn siRNA-MEND group compared with the control group (Figure 5F,G).

Furthermore, we analyzed hypoxic condition in the tumors. GLUT1 is one of the hypoxia markers regulated by HIF-1.[44,45] GLUT1 staining data indicated that the hypoxia area was reduced by Bgn siRNA-MEND treatment (Figure 5H,I). Fibrosis is one of the important factors for tumor malignancy. Azan staining revealed that collagen accumulation in the Bgn siRNA-MEND group was lower than that in the control group (Figure 5J,K), suggesting that fibrosis was diminished by biglycan inhibition.

4 | DISCUSSION

Biglycan, highly expressed in TECs, is involved in tumor angiogenesis and metastasis, thereby demonstrating significant potential as a
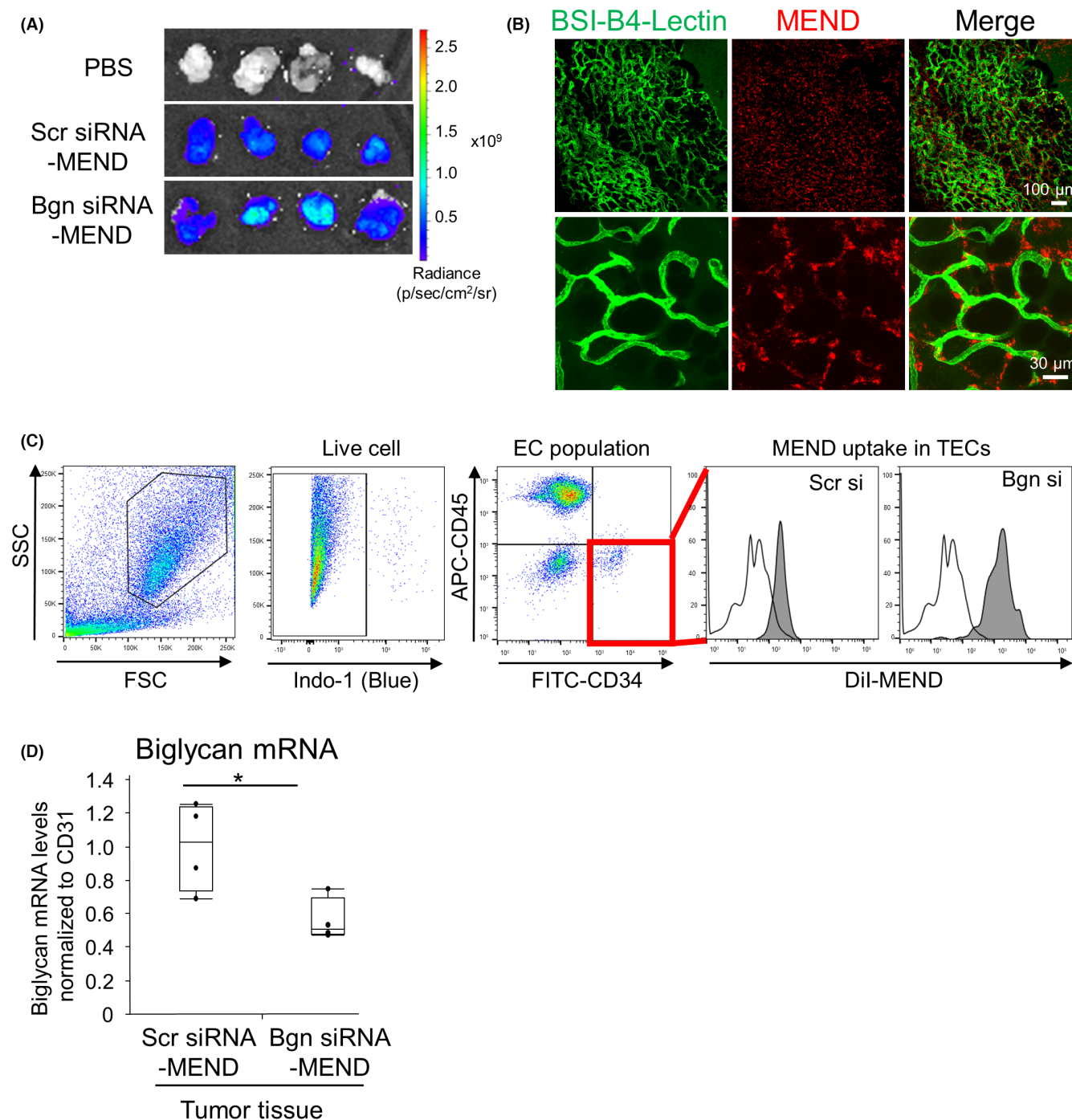
FIGURE 3 Uptake and gene silencing by MEND in OS-RC-2-ECs were evaluated *in vivo*. (A) Each MEND fluorescence intensity in the tumors was detected using the IVIS Spectrum system 24 h after the second MEND injection. Notably, each siRNA-MEND was accumulated in tumor tissues. (B) All blood vessels in tumors were visualized by staining of the resected tumors with FITC-BSI-B4 lectin. Specimens were observed under a fluorescence microscope. Notably, MEND (red) signals were colocalized with FITC-BSI-B4 lectin (green). Upper, low magnification; lower, high magnification. (C) Representative flow cytometric analysis of MEND uptake in the ECs of OS-RC-2 tumor tissues. CD34$^+$CD45$^-$ populations in OS-RC-2 tumors were defined as TECs. TECs that uptake each MEND are shown as a gray expression area. ECs from tumors that are treated with vehicle instead of MEND were used as control (white area). (D) Biglycan expression in each tumor group was evaluated by qRT-PCR (*$p < 0.01$, two-tailed Student's *t* test; $n = 4$). CD31 was used as an internal control to normalize the amount of ECs

possible target for anticancer therapy. However, targeting biglycan for therapy has not yet been reported because there are no commercially available inhibitors for biglycan. In this study, we developed a TEC-targeting nano DDS system to target biglycan in TECs. The TEC-targeting MEND was delivered into TECs, therefore inhibiting biglycan expression both *in vitro* and *in vivo*. Biglycan inhibition using

FIGURE 4 Antitumor effect by Bgn siRNA-MEND. (A) Schematic of MEND treatment: Scr siRNA-MEND or Bgn siRNA-MEND was intravenously injected into OS-RC-2-bearing mice twice a week for 3 weeks beginning on day 7 (n = 4). (B) Mouse body weight in each group was measured. No notable difference was observed between the two groups. NS, not significant. (C) Images of whole tumors resected from mice under each treatment condition at day 28. Scale bar, 1 cm. (D) Tumor weight in each group was measured (*$p < 0.05$, two-tailed Student's t test; n = 4)
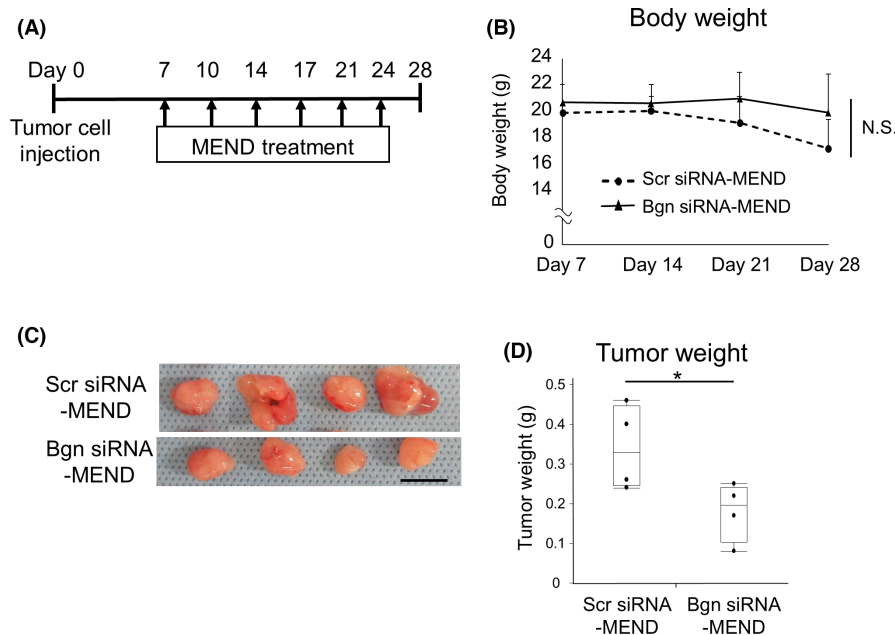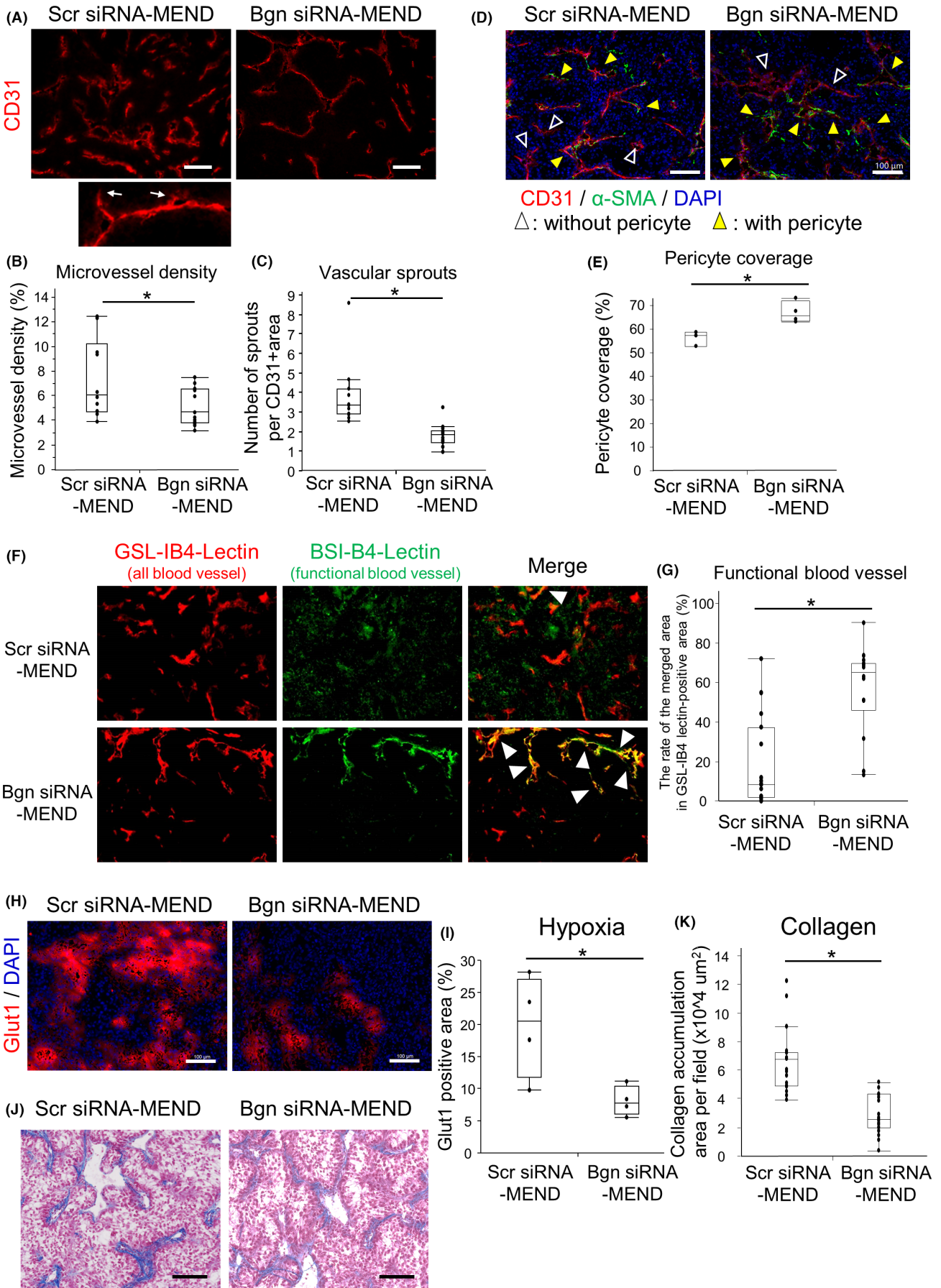
MEND resulted in not only antiangiogenesis but also normalization of the tumor microenvironment, with increase in pericyte coverage and blood perfusion, decrease in hypoxia area, and reduction of fibrosis. Our results provided clear evidence that biglycan is a good target for cancer therapy.

Biglycan is a member of the class I small leucine-rich proteoglycan consisting of a 42-kDa protein core and one or two covalently linked glycosaminoglycan chains at its N-terminus.[46] It is expressed in the ECM and plays a key role as a matrix component and essential signaling molecule.[19] Biglycan has been considered as a potential anticancer target due to its high expression in various cancers.[47] High-level biglycan expression is associated with poor prognosis in gastric cancer,[48] colorectal cancer,[49] bladder cancer,[50,51] endometrial cancer,[52] melanoma,[42] and prostate cancer.[53] Biglycan overexpression in gastric cancer cell lines was found to activate their migration, invasion, and peritoneal spreading through focal adhesion kinase signaling.[54] In colon cancer cell lines, biglycan overexpression promoted chemoresistance using activating NF-κB.[55] Recombinant biglycan treatment was found to facilitate tumor cell migration through the TLR/NF-κB/HIF1-α/VEGF-mediated axis.[21,56] Our previous analysis of biglycan expression in human tissues of renal cancer, lung cancer, colon cancer, and liver tumor by immunohistochemistry showed that most biglycan signals were detected in tumor blood vessels.[14,21,57] Our earlier research also demonstrated the role of biglycan in ECs, for which we observed that the migration and tube formation of TECs were inhibited by biglycan knockdown with its siRNA through TLRs.[14] It has also been reported that biglycan induces VEGF expression through the TLR/NF-κB/HIF1-α[56] or the extracellular signal-regulated kinase signaling pathway in ECs.[58] Recently, we found that biglycan knockout in the stroma of breast cancer-bearing mice inhibited metastasis to the lung, impaired tumor angiogenesis, normalized the tumor vasculature, improved the delivery of chemotherapeutic drugs and CD8+ T-cell infiltration, and suppressed fibrosis.[22] In the present study, biglycan was expressed in tumors, including blood vessels. The effect of biglycan inhibition using the DDS system was consistent with our previous findings. The abundance of biglycan affects several cell types in the tumor microenvironment as it is a secreted protein.

Angiogenesis is required for tumor growth and metastasis. To cut off blood supply, antiangiogenic therapy was widely used for cancer therapy. However, it sometimes causes severe adverse effects such as intestinal perforation[59] due to normal blood vessel damage. Specific targeting and delivery of therapeutics to tumor blood vessels would be an ideal strategy. Several research groups, including ours, have found that some genes are upregulated in TECs compared with NECs.[6–11] Those molecules can be candidates for TEC-targeting therapy. Specifically, another strategy is delivering a drug into tumor blood vessels using the nano DDS system. Because TECs face toward the bloodstream, TECs are easily accessed using intravenously administered nano DDS. Most solid tumors exhibit enhanced vascular permeability due to the defective architecture of blood vessels and the production of excessive amounts of several vascular permeability factors such as VEGF. In addition to nutrients and oxygen, drugs are passively accumulated in tumor tissues. This phenomenon is known as the enhanced permeability and retention effect[60] and has been the gold standard in anticancer strategies, and several drugs are delivered through blood vessels. However, we must develop active targeting nanoparticles to specifically deliver nano DDS to TECs. For delivering active targeting nano DDS into TECs, several ligands, such as peptides, sugars, and nucleic acid aptamers, have been reported.[61] In this study, cRGD is used. The RGD motif is recognized by integrin heterodimers between the α_V unit and β_3 unit, and it can specifically bind with those cells because integrin $\alpha_V\beta_3$ is expressed in TECs and some cancer cell types. In this study, we used a nano DDS system, MEND, which is an siRNA-loaded lipid nanoparticle, using a pH-responsive cationic lipid, YSK05, as

(A) Scr siRNA-MEND   Bgn siRNA-MEND
CD31

(B) Microvessel density
(C) Vascular sprouts
(D) Scr siRNA-MEND   Bgn siRNA-MEND
CD31 / α-SMA / DAPI
△: without pericyte   ▲ : with pericyte

(E) Pericyte coverage

(F) GSL-IB4-Lectin (all blood vessel)   BSI-B4-Lectin (functional blood vessel)   Merge
Scr siRNA-MEND
Bgn siRNA-MEND

(G) Functional blood vessel

(H) Scr siRNA-MEND   Bgn siRNA-MEND
Glut1 / DAPI

(I) Hypoxia
(J) Scr siRNA-MEND   Bgn siRNA-MEND
(K) Collagen

FIGURE 5 Therapeutic effect of biglycan inhibition by MEND. (A) Representative images of tumor sections fixed and stained with anti-CD31 antibody (red) to identify the blood vessels. The lower panel shows an enlarged image with tip-like endothelial sprouts (arrow). Scale bars, 100 μm. (B) Tumor microvessel density was analyzed by quantifying the CD31-positive stained area in tumor sections from each group using ImageJ software (*$p < 0.05$ versus Scr siRNA-MEND-treated group, two-tailed Student's t test; $n = 4$ fields per mouse). (C) The number of tip-like endothelial sprouts per CD31-positive area (pixel) was calculated in tumor sections from each group. Tip-like endothelial sprouts were defined as tapered endothelial processes that extended from the main axis of vessels (*$p < 0.05$ versus Scr siRNA-MEND-treated group, two-tailed Student's t test; $n = 4$ fields per mouse). (D) Tumor blood vessels and pericytes were stained with anti-CD31 (red) and anti-α-SMA (green) antibodies, respectively, and counterstained with DAPI (blue). Scale bars, 100 μm. (E) The rate of microvessel pericyte coverage was analyzed by counting the vessels that stained positively for both CD31 and α-SMA (yellow arrowheads) among all CD31-positive vessels. The outline in white indicates α-SMA-negative vessels (*$p < 0.05$ versus Scr siRNA-MEND-treated group, two-tailed Student's t test; $n = 4$ fields per mouse). (F) Functional blood vessels in the tumors were visualized by intravenously injecting Alexa Fluro647-conjugated GSL-IB4 lectin, and all blood vessels in tumors were visualized by staining the resected tumors with FITC-BSI-B4 lectin. Specimens were observed under a fluorescence microscope. Arrowheads indicate colocalization. (G) Functional blood vessels were calculated as the rate of the merged area in GSL-IB4 lectin-positive area in tumor sections from each group using ImageJ software (*$p < 0.01$ versus Scr siRNA-MEND-treated group, two-tailed Student's t test; $n = 15$ fields per group). (H) Representative images of tumor sections fixed and stained with anti-GLUT1 antibody (red) to identify the hypoxia area. Scale bars, 100 μm. (I) Hypoxia area was analyzed by quantifying the GLUT1-positive stained area in tumor sections from each group using ImageJ software (*$p < 0.05$ versus Scr siRNA-MEND-treated group, two-tailed Student's t test; $n = 4$ fields per mouse). (J) Azan staining was performed in each tumor section. The cytoplasm and collagen fibers are stained orange and blue, respectively. Scale bars, 100 μm. (K) Collagen accumulation was analyzed by quantifying the collagen-positive stained area in tumor sections from each group using ImageJ software (*$p < 0.01$ versus Scr siRNA-MEND-treated group, two-tailed Student's t test; $n = 5$ fields per mouse)

developed previously.[28,29] To target TECs, MEND was modified with cRGD through the postmodification of cRGD-PEG-lipid conjugates.[31] We previously confirmed that the siRNA-encapsulating RGD-MEND was specifically delivered into integrin-positive human umbilical vein ECs but not into HEK293T cells.[31] Additionally, in this study, we confirmed the integrin expression and uptake of RGD-MEND in TECs (Figure 2). Also, the selective delivery of the siRNA RGD-MEND to tumor tissues, especially in TECs, was proven using flow cytometric analysis (Figure S3). We previously observed the effect of doxorubicin-loaded RGD-MEND in blood vessels of OS-RC-2 tumor-bearing mice. We found that apoptotic cells were observed in the tumor vessels, but the morphology of blood vessels in the normal liver, spleen, and lung tissue showed no unusual morphological alteration.[62] In addition to this previous report, doxorubicin did not affect normal blood vessels by RGD-MEND, even though normal ECs in normal tissue, such as kidney and skin, take up the biglycan siRNA-MEND, their harmful effects might be low because of their low biglycan expression (Figure 1B). Moreover, we previously confirmed gene silencing by siRNA-DDS using qRT-PCR and rapid amplification of 5′ cDNA ends (5′RACE-PCR),[31] which was the only available method to confirm RNAi-induced silencing.[63] The RGD-MEND-encapsulating anti-VEGFR2 siRNA significantly inhibited tumor growth[31] and improved poor intratumor nanoparticle distribution.[32,38] It is well known that, because the loose interconnections of endothelial cells in tumor blood vessels result in high interstitial fluid pressure, tumor blood vessels are collapsed, and blood flow is impeded. In this study, MEND signals were detected in nonfunctional blood vessels 24 h after a single MEND injection (Figure S3B). The efficacy of biglycan knockdown was limited in this study by the siRNA-MEND. However, ghost blood vessels without active blood flow may affect siRNA-DDS delivery. Several injections or further delivery system development would increase biglycan inhibition and their therapeutic effects.

The reasons for our selection of a renal cell carcinoma model for the present study are as follows: renal cell carcinoma is an angiogenic tumor, antiangiogenic therapy is approved in cancer treatment, and we found in our previous study that biglycan is upregulated in the TECs of human renal cell carcinoma.[14] In clinical therapy, single antiangiogenic drug treatment does not completely eliminate cancers; similarly, single biglycan knockdown by nucleic acid medicine using MEND was not sufficient to completely heal the tumor. Furthermore, combination therapy with some anticancer drugs may be required as there are several proangiogenic factors in addition to biglycan. Recently, vascular normalization was also proposed as an alternative effect of antiangiogenic therapy. Antiangiogenic therapy normalizes the abnormal structure and function of the tumor vasculature to achieve more efficient oxygen and drug delivery.[64] We showed that biglycan inhibition by MEND increased the pericyte-covered blood vessels and improved blood perfusion and hypoxic conditions, which is one of the characteristics of vascular normalization. Drug delivery can be improved by biglycan inhibition, and further studies are required to verify the efficacy of biglycan inhibition as a combination therapy. Antiangiogenic therapy is also expected to improve the efficacy of immunotherapy.[65] There exists a possibility that biglycan inhibition can improve the efficacy of immune checkpoint inhibitors, because blood flow improvement is beneficial for immune cells to distribute in tumor tissues. However, in this study, nude mice were used to apply the human renal cancer cell line. Nude mice lack a thymus that causes T-cell deficiency, which limits this study in confirming the efficacy of biglycan inhibition in immune cells; therefore, further studies using syngeneic models are required. Fibrosis in the tumor microenvironment is one of the causes of tumor progression. Stiffened stroma enhances tumor cell growth, survival, and migration.[66] Tumor fibrosis results in a poor response to anticancer therapy. Decreasing fibrosis through biglycan inhibition can also be effective for cancer therapy. To summarize,

targeting biglycan can induce an antitumor effect, antiangiogenic effect, normalization of tumor blood vessels, and decreased fibrosis in tumors. Therefore, biglycan inhibition as a strategy for cancer therapy may have multiple efficacies.

DISCLOSURE

There are no financial or other relations that could lead to a conflict of interest regarding this study. H Harashima and K Hida are current Editorial Board members of Cancer Science.

ORCID

Hiroto Hatakeyama https://orcid.org/0000-0003-3899-0508
Takashi Nakamura https://orcid.org/0000-0001-9019-1426
Hiroshi Kikuchi https://orcid.org/0000-0003-4999-8994
Yasuhiro Hida https://orcid.org/0000-0003-1759-4215
Kyoko Hida https://orcid.org/0000-0002-7968-6062

REFERENCES

1. Proceedings FJ. Tumor angiogenesis factor. *Cancer Res*. 1974;34:2109-2113.
2. Folkman J. Anti-angiogenesis: new concept for therapy of solid tumors. *Ann Surg*. 1972;175:409-416.
3. Ferrara N, Hillan KJ, Novotny W. Bevacizumab (Avastin), a humanized anti-VEGF monoclonal antibody for cancer therapy. *Biochem Biophys Res Commun*. 2005;333:328-335.
4. Chen HX, Cleck JN. Adverse effects of anticancer agents that target the VEGF pathway. *Nat Rev Clin Oncol*. 2009;6:465-477.
5. Hida K, Maishi N, Torii C, Hida Y. Tumor angiogenesis–characteristics of tumor endothelial cells. *Int J Clin Oncol*. 2016;21:206-212.
6. St Croix B, Rago C, Velculescu V, et al. Genes expressed in human tumor endothelium. *Science*. 2000;289:1197-1202.
7. Langenkamp E, Molema G. Microvascular endothelial cell heterogeneity: general concepts and pharmacological consequences for anti-angiogenic therapy of cancer. *Cell Tissue Res*. 2009;335:205-222.
8. Arap W, Kolonin MG, Trepel M, et al. Steps toward mapping the human vasculature by phage display. *Nat Med*. 2002;8:121-127.
9. Trepel M, Arap W, Pasqualini R. In vivo phage display and vascular heterogeneity: implications for targeted medicine. *Curr Opin Chem Biol*. 2002;6:399-404.
10. Hida K, Hida Y, Amin DN, et al. Tumor-associated endothelial cells with cytogenetic abnormalities. *Cancer Res*. 2004;64:8249-8255.
11. Otsubo T, Hida Y, Ohga N, et al. Identification of novel targets for antiangiogenic therapy by comparing the gene expressions of tumor and normal endothelial cells. *Cancer Sci*. 2014;105:560-567.
12. Matsuda K, Ohga N, Hida Y, et al. Isolated tumor endothelial cells maintain specific character during long-term culture. *Biochem Biophys Res Commun*. 2010;394:947-954.
13. Ohga N, Ishikawa S, Maishi N, et al. Heterogeneity of tumor endothelial cells: comparison between tumor endothelial cells isolated from high- and low-metastatic tumors. *Am J Pathol*. 2012;180:1294-1307.
14. Yamamoto K, Ohga N, Hida Y, et al. Biglycan is a specific marker and an autocrine angiogenic factor of tumour endothelial cells. *Br J Cancer*. 2012;106:1214-1223.
15. Osawa T, Ohga N, Hida Y, et al. Prostacyclin receptor in tumor endothelial cells promotes angiogenesis in an autocrine manner. *Cancer Sci*. 2012;103:1038-1044.
16. Alam MT, Nagao-Kitamoto H, Ohga N, et al. Suprabasin as a novel tumor endothelial cell marker. *Cancer Sci*. 2014;105:1533-1540.
17. Osawa T, Ohga N, Akiyama K, et al. Lysyl oxidase secreted by tumour endothelial cells promotes angiogenesis and metastasis. *Br J Cancer*. 2013;109:2237-2247.
18. Yamada K, Maishi N, Akiyama K, et al. CXCL12-CXCR7 axis is important for tumor endothelial cell angiogenic property. *Int J Cancer*. 2015;137:2825-2836.
19. Nastase MV, Young MF, Schaefer L. Biglycan: a multivalent proteoglycan providing structure and signals. *J Histochem Cytochem*. 2012;60:963-975.
20. Schaefer L, Babelova A, Kiss E, et al. The matrix component biglycan is proinflammatory and signals through Toll-like receptors 4 and 2 in macrophages. *J Clin Invest*. 2005;115:2223-2233.
21. Maishi N, Ohba Y, Akiyama K, et al. Tumour endothelial cells in high metastatic tumours promote metastasis via epigenetic dysregulation of biglycan. *Sci Rep*. 2016;6:28039.
22. Cong L, Maishi N, Annan DA, et al. Inhibition of stromal biglycan promotes normalization of the tumor microenvironment and enhances chemotherapeutic efficacy. *Breast Cancer Res*. 2021;23:51.
23. Whitehead KA, Langer R, Anderson DG. Knocking down barriers: advances in siRNA delivery. *Nat Rev Drug Discov*. 2009;8:129-138.
24. Catuogno S, Esposito CL, Condorelli G, de Franciscis V. Nucleic acids delivering nucleic acids. *Adv Drug Deliv Rev*. 2018;134:79-93.
25. Sakurai Y, Kajimoto K, Hatakeyama H, Harashima H. Advances in an active and passive targeting to tumor and adipose tissues. *Expert Opin Drug Deliv*. 2015;12:41-52.
26. Kogure K, Akita H, Yamada Y, Harashima H. Multifunctional envelope-type nano device (MEND) as a non-viral gene delivery system. *Adv Drug Deliv Rev*. 2008;60:559-571.
27. Hatakeyama H, Akita H, Harashima H. A multifunctional envelope type nano device (MEND) for gene delivery to tumours based on the EPR effect: a strategy for overcoming the PEG dilemma. *Adv Drug Deliv Rev*. 2011;63:152-160.
28. Sato Y, Hatakeyama H, Sakurai Y, Hyodo M, Akita H, Harashima H. A pH-sensitive cationic lipid facilitates the delivery of liposomal siRNA and gene silencing activity *in vitro* and *in vivo*. *J Control Release*. 2012;163:267-276.
29. Sakurai Y, Hatakeyama H, Sato Y, Hyodo M, Akita H, Harashima H. Gene silencing via RNAi and siRNA quantification in tumor tissue using MEND, a liposomal siRNA delivery system. *Mol Ther*. 2013;21:1195-1203.
30. Avraamides CJ, Garmy-Susini B, Varner JA. Integrins in angiogenesis and lymphangiogenesis. *Nat Rev Cancer*. 2008;8:604-617.
31. Sakurai Y, Hatakeyama H, Sato Y, et al. RNAi-mediated gene knockdown and anti-angiogenic therapy of RCCs using a cyclic RGD-modified liposomal-siRNA system. *J Control Release*. 2014;173:110-118.
32. Yamamoto S, Kato A, Sakurai Y, Hada T, Harashima H. Modality of tumor endothelial VEGFR2 silencing-mediated improvement in intratumoral distribution of lipid nanoparticles. *J Control Release*. 2017;251:1-10.
33. Akino T, Hida K, Hida Y, et al. Cytogenetic abnormalities of tumor-associated endothelial cells in human malignant tumors. *Am J Pathol*. 2009;175:2657-2667.
34. Tsuchiya K, Hida K, Hida Y, et al. Adrenomedullin antagonist suppresses tumor formation in renal cell carcinoma through inhibitory effects on tumor endothelial cells and endothelial progenitor mobilization. *Int J Oncol*. 2010;36:1379-1386.
35. Maishi N, Ohga N, Hida Y, et al. CXCR7: a novel tumor endothelial marker in renal cell carcinoma. *Pathol Int*. 2012;62:309-317.

36. Akiyama K, Ohga N, Maishi N, et al. The F-prostaglandin receptor is a novel marker for tumor endothelial cells in renal cell carcinoma. *Pathol Int*. 2013;63:37-44.

37. Sakurai Y, Hada T, Harashima H. Preparation of a cyclic RGD: modified liposomal sirna formulation for use in active targeting to tumor and tumor endothelial cells. *Methods Mol Biol*. 2016; 1364:63-69.

38. Sakurai Y, Hada T, Yamamoto S, Kato A, Mizumura W, Harashima H. Remodeling of the extracellular matrix by endothelial cell-targeting siRNA improves the EPR-based delivery of 100 nm particles. *Mol Ther*. 2016;24:2090-2099.

39. Sakurai Y, Hatakeyama H, Akita H, Harashima H. Improvement of doxorubicin efficacy using liposomal anti-polo-like kinase 1 siRNA in human renal cell carcinomas. *Mol Pharm*. 2014;11: 2713-2719.

40. Morikawa S, Baluk P, Kaidoh T, Haskell A, Jain RK, McDonald DM. Abnormalities in pericytes on blood vessels and endothelial sprouts in tumors. *Am J Pathol*. 2002;160:985-1000.

41. Hashizume H, Falcon BL, Kuroda T, et al. Complementary actions of inhibitors of angiopoietin-2 and VEGF on tumor angiogenesis and growth. *Cancer Res*. 2010;70:2213-2223.

42. Andrlova H, Mastroianni J, Madl J, et al. Biglycan expression in the melanoma microenvironment promotes invasiveness via increased tissue stiffness inducing integrin-beta1 expression. *Oncotarget*. 2017;8:42901-42916.

43. Zheng S, Zou Y, Tang Y, et al. Landscape of cancer-associated fibroblasts identifies the secreted biglycan as a protumor and immunosuppressive factor in triple-negative breast cancer. *Oncoimmunology*. 2022;11:2020984.

44. Little RA, Jamin Y, Boult JKR, et al. Mapping hypoxia in renal carcinoma with oxygen-enhanced MRI: Comparison with Intrinsic susceptibility MRI and pathology. *Radiology*. 2018;288:739-747.

45. Hoskin PJ, Sibtain A, Daley FM, Wilson GD. GLUT1 and CAIX as intrinsic markers of hypoxia in bladder cancer: relationship with vascularity and proliferation as predictors of outcome of ARCON. *Br J Cancer*. 2003;89:1290-1297.

46. Bianco P, Fisher LW, Young MF, Termine JD, Robey PG. Expression and localization of the two small proteoglycans biglycan and decorin in developing human skeletal and non-skeletal tissues. *J Histochem Cytochem*. 1990;38:1549-1563.

47. Appunni S, Anand V, Khandelwal M, Gupta N, Rubens M, Sharma A. Small Leucine Rich Proteoglycans (decorin, biglycan and lumican) in cancer. *Clin Chim Acta*. 2019;491:1-7.

48. Wang B, Li GX, Zhang SG, et al. Biglycan expression correlates with aggressiveness and poor prognosis of gastric cancer. *Exp Biol Med (Maywood)*. 2011;236:1247-1253.

49. Gu X, Ma Y, Xiao J, et al. Up-regulated biglycan expression correlates with the malignancy in human colorectal cancers. *Clin Exp Med*. 2012;12:195-199.

50. Niedworok C, Rock K, Kretschmer I, et al. Inhibitory role of the small leucine-rich proteoglycan biglycan in bladder cancer. *PLoS One*. 2013;8:e80084.

51. Appunni S, Anand V, Khandelwal M, Seth A, Mathur S, Sharma A. Altered expression of small leucine-rich proteoglycans (Decorin, Biglycan and Lumican): Plausible diagnostic marker in urothelial carcinoma of bladder. *Tumour Biol*. 2017;39:1010428317699112.

52. Liu Y, Li W, Li X, et al. Expression and significance of biglycan in endometrial cancer. *Arch Gynecol Obstet*. 2014;289:649-655.

53. Jacobsen F, Kraft J, Schroeder C, et al. Up-regulation of biglycan is associated with poor prognosis and PTEN deletion in patients with prostate cancer. *Neoplasia*. 2017;19:707-715.

54. Hu L, Duan YT, Li JF, et al. Biglycan enhances gastric cancer invasion by activating FAK signaling pathway. *Oncotarget*. 2014;5:1885-1896.

55. Liu B, Xu T, Xu X, Cui Y, Xing X. Biglycan promotes the chemotherapy resistance of colon cancer by activating NF-kappaB signal transduction. *Mol Cell Biochem*. 2018;449:285-294.

56. Hu L, Zang MD, Wang HX, et al. Biglycan stimulates VEGF expression in endothelial cells by activating the TLR signaling pathway. *Mol Oncol*. 2016;10:1473-1484.

57. Morimoto H, Hida Y, Maishi N, et al. Biglycan, tumor endothelial cell secreting proteoglycan, as possible biomarker for lung cancer. *Thorac Cancer*. 2021;12(9):1347-1357.

58. Xing X, Gu X, Ma T, Ye H. Biglycan up-regulated vascular endothelial growth factor (VEGF) expression and promoted angiogenesis in colon cancer. *Tumour Biol*. 2015;36:1773-1780.

59. Frandsen S, Kopp S, Wehland M, Pietsch J, Infanger M, Grimm D. Latest results for anti-angiogenic drugs in cancer treatment. *Curr Pharm Des*. 2016;22:5927-5942.

60. Matsumura Y, Maeda H. A new concept for macromolecular therapeutics in cancer chemotherapy: mechanism of tumoritropic accumulation of proteins and the antitumor agent smancs. *Cancer Res*. 1986;46:6387-6392.

61. Sakurai Y, Akita H, Harashima H. Targeting tumor endothelial cells with nanoparticles. *Int J Mol Sci*. 2019;20(23):5819.

62. Kibria G, Hatakeyama H, Ohga N, Hida K, Harashima H. The effect of liposomal size on the targeted delivery of doxorubicin to Integrin alphavbeta3-expressing tumor endothelial cells. *Biomaterials*. 2013;34:5617-5627.

63. Rettig GR, Behlke MA. Progress toward *in vivo* use of siRNAs-II. *Mol Ther*. 2012;20:483-512.

64. Jain RK. Normalization of tumor vasculature: an emerging concept in antiangiogenic therapy. *Science*. 2005;307:58-62.

65. Allen E, Jabouille A, Rivera LB, et al. Combined antiangiogenic and anti-PD-L1 therapy stimulates tumor immunity through HEV formation. *Sci Transl Med*. 2017;9(385).

66. Piersma B, Hayward MK, Weaver VM. Fibrosis and cancer: A strained relationship. *Biochim Biophys Acta Rev Cancer*. 2020;1873:188356.

SUPPORTING INFORMATION

Additional supporting information may be found in the online version of the article at the publisher's website.